Tetrahedron 73 (2017) 1551–1560

Contents lists available at ScienceDirect

Tetrahedron

journal homepage: www.elsevier.com/locate/tet

Assessing stereoelectronic effects in dipolar cycloadditions yielding fused thiazolopyridone rings

Juan García de la Concepción [a, *], Martín Ávalos [a], Reyes Babiano [a], Pedro Cintas [a, **], José L. Jiménez [a], Mark E. Light [b], Juan C. Palacios [a]

[a] Departamento de Química Orgánica e Inorgánica, Facultad de Ciencias and IACYS-Unidad de Química Verde y Desarrollo Sostenible, Universidad de Extremadura, E-06006, Badajoz, Spain
[b] Department of Chemistry, Faculty of Natural and Environmental Sciences, University of Southampton, Southampton, SO17 1BJ, UK

ARTICLE INFO

Article history:
Received 9 December 2016
Received in revised form
17 January 2017
Accepted 26 January 2017
Available online 5 February 2017

Keywords:
Thioisomünchnone
Cycloaddition
Natural bond orbital (NBO)
Natural localized molecular orbital (NLMO)
Natural steric analysis (NSA)
Natural bond critical point (NBCP)

ABSTRACT

We report a combined experimental and computational study on the cycloadditions of bicyclic 1,3-thiazolium-4-olates, derived from thiazolidin-2-thiones, with asymmetrically-substituted acetylenes. These results provide further mechanistic insights into the above dipolar cycloadditions and enable an unequivocal characterization by NMR spectroscopy of regiochemical patterns as previous derivatives had substituents at both C-2 (in the dipole) and C-6 (in products). Accordingly, new dihydrothiazolopyrid-2-ones have been obtained from a thioisomünchnone lacking substitution at C-2. With the aim of assessing the steric hindrance as well as the facial stereoselection induced by a bulky group on the *Si* face (relative to C-7a) of the mesoionic heterocycle, a chiral thioisomünchnone has also been obtained along with the resulting optically active thiazolopyridones. A computational study of these particular cycloadditions, largely based on an NBO analysis, allowed us to evaluate the influence of substituents on intermolecular steric repulsions, charge transfers, as well as solvent effects.

1. Introduction

Fused heterocycles comprising five- and six-membered rings, usually containing a ring-junction nitrogen, are privileged scaffolds in medicinal chemistry and such systems are frequently employed to assess and develop compound libraries and new leads.[1,2] Among them, thiazolopyridine derivatives in particular have gained some attention as potential drug candidates against different pathologies.[3,4]

The synthesis of densely functionalized heteroatom-containing rings may be accomplished by different strategies, although shortcuts often rely on [3 + 2]-cycloadditions as well as multi-component reactions capable of assembling the two-unit framework in chemo- and regio-controlled fashions.[5,6] Facile and versatile elaborations harness the pentagonal core of mesoionic heterocycles, which behaving as masked allyl-type dipoles, enable further structural fusion and/or elongation with appropriate dipolarophiles, usually in metal-free protocols.[7,8] Mesoionic-based dipolar cycloadditions actually give rise to a variety of heterocyclic arrays not easily provided by conventional cycloadditions, as developed by our group over the last two decades.[9]

Recently, we have described the synthesis of a new fused-ring thioisomünchnone (**1**) and its 1,3-dipolar reactivity toward activated acetylenes, with a focus on the sulfur extrusion mechanism,[10] which constitutes the key step in the chemoselective syntheses of pyridin-2-ones or thiophenes from the above mesoionic rings. Despite some controversial results in the literature claiming either concerted retro-cheletropic reactions or stepwise pathways for the spontaneous loss of sulfur, or isocyanate, from the resulting monoadducts formed initially in the cycloadditions of thioisomünchnones with alkynes, that study unveiled a sigmatropic mechanism involving the intermediacy of thiirane species. Moreover, the regioselective addition of asymmetrically-substituted acetylenes to the mesoionic heterocycle (*e.g.* by reaction of **1** with methyl propiolate) could be corroborated by single-crystal X-ray diffractometry of compound **2** and further rationalized by DFT analysis.[10] Unfortunately, in the absence of unequivocal crystal data, the regiochemical outcome leading spontaneously to thiazolo[3,2-*a*]pyridine-5-ones cannot easily be monitored. A phenyl group

* Corresponding author.
** Corresponding author.
E-mail addresses: jugarco@unex.com (J.G. de la Concepción), pecintas@unex.es (P. Cintas).

http://dx.doi.org/10.1016/j.tet.2017.01.064
0040-4020/

at C-2 in **1**, and therefore in C-6 in **2** and its analogous, limits the diagnostic use of NMR signals to this end. To overcome this hurdle, the present study reports the synthesis and cycloadditions of an unsubstituted derivative, namely 5,6-dihydrothiazolo[2,3-*b*]thiazol-4-ium-3-olate (**3**), which not only allows the straightforward inspection of the regiochemical pattern by proton NMR, but also evaluates the influence, if any, of the substituent at C-2. Furthermore, a chiral thioisomünchnone (**15**) bearing a bulky and inert group was obtained to check, if any, the issue of facial selection. Although, as we shall see, the latter cannot be assessed from an experimental point of view, the computational study still unveils how such a facial stereodiscrimination would take place and the influence exerted by the dipolarophile's structure in particular.

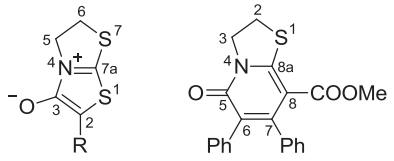

1 R = Ph
3 R = H

2

2. Results and discussion

2.1. Synthesis and structural characterization

In principle the preparation of **3** should proceed by a similar procedure to that described for the preparation of **1**, using bromoacetic acid as alkylating reagent of thiazolidine-2-thione (**4**). The intermediate thioglycolic acid, i.e. 2-[(4,5-dihydrothiazol-2-yl)thio] acetic acid (**5**) could be isolated as a white solid in good yield (>90%). However, unlike the synthesis of **1**, conventional cyclodehydration of **5** with Ac_2O/Et_3N (1:3 ratio) did not afford **3** as a stable solid. Thus, we devised a one-pot protocol that generates **3** *in situ* in the presence of acetylenes **6**–**8** leading to 8-alkoxycarbonyl-5-oxo-3,5-dihydro-2*H*-thiazolo[3,2-*a*]pyridines (**9**–**11**) (Scheme 1).

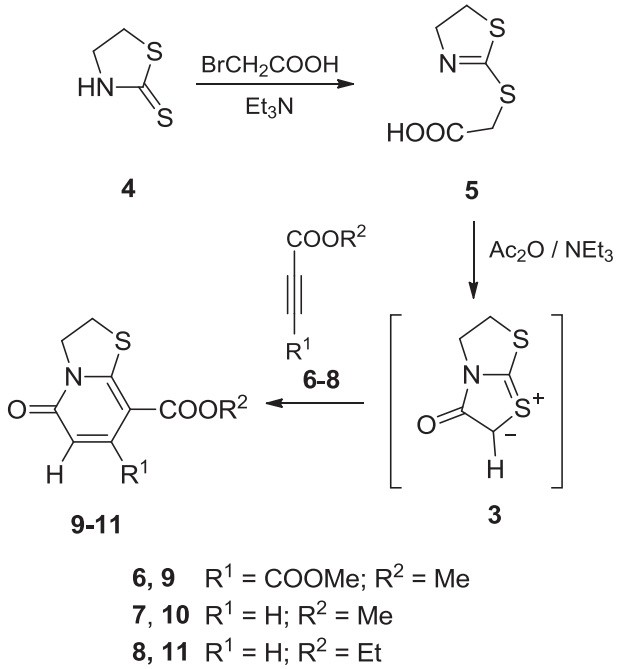

Scheme 1. Synthesis of thiazolo[3,2-*a*]pyridines **9**–**11** by dipolar cycloaddition of a transient dipole (**3**), generated from **5**, with acetylenes.

The above thermal cycloaddition could easily be carried out by mixing **5** and the corresponding dipolarophile (1:1.5 ratio) in CH_2Cl_2, then adding dropwise a mixture of acetic anhydride and triethylamine (1:3), and finally heated at reflux for 1 h. Chromatographic purification gave rise to compounds **9**–**11** in variable and rather modest yields (15–37%). ^{1}H NMR spectra of **10** and **11** were quite similar and showed two doublet signals at δ ~7.8 and ~6.2 ppm (J = 9.5 Hz) assignable to vicinal H-6 and H-7 protons, respectively.

As mentioned in the introductory remarks, with the aim of evaluating the role of steric effects as well as the facial stereoselection induced by a bulky substituent located on the *Si* face (relative to C-7a) of the mesoionic heterocycle, the chiral thioisomünchnone **15** derived from (*S*)-4-isopropylthiazolidine-2-thione (**13**) and α-bromophenylacetic acid was prepared. Compound **13** has been previously obtained by reaction of (*S*)-2-amino-3-methylbutan-1-ol (**12**) with CS_2 in alkaline solution (KOH).[11] The resulting (*S*)-5-isopropyl-2-phenyl-5,6-dihydrothiazolo[2,3-*b*]thiazol-4-ium-3-olate (**15**) could be obtained by treating the mixture containing **14** (not isolated) with Ac_2O/Et_3N (Scheme 2).

Reactions of **15** with dipholarophiles **6**–**8** were conducted in toluene at reflux using an excess of dipolarophile (25%) and the end point could be easily determined after the complete disappearance of the characteristic orange color of the mesoionic heterocycle (~2 h). The solvent was removed under reduced pressure and the residue treated with methanol to give pure (*S*)-3-isopropyl-5-oxo-6-phenyl-3,5-dihydro-2*H*-thiazolo[3,2-*a*]pyridines **16**–**18** in moderate to good overall yields (54–75%). It should be noted that inspection of crude mixtures by NMR spectroscopy prior to purification gave no evidence of any other regioisomer. Moreover, no signals accounting for the competitive formation of thiophenes or isocyanates as side products could be observed either. The modest yields of thiazolopyridones **9**–**11** in particular, as well as of **16**–**18** largely result from the thermal lability of the mesoionic dipole. Thiazolopyridone **16** enables a rapid structural elucidation by NMR and, gratifyingly compound **17** could be unambiguously characterized by single-crystal X-ray diffraction (Fig. 1).[12]

2.2. Mechanistic insights on the dipolar cycloaddition

As reported previously,[10] the reaction of **1** with methyl propiolate (**7**) in toluene involves initially a regiospecific stepwise 1,3-dipolar cycloaddition (rate-determining step) (Scheme 3). The initial cycloadduct then undergoes a 1,3-sigmatropic rearrangement to give a transient thiirane, which ultimately extrudes sulfur through a 1,2-elimination leading to pyridone **19** (for a detailed picture of the reaction pathways, see Figures S1–S3).

A comparison of the energetic profiles for the cycloadditive steps of thioisomünchnones **1** and **3** with **7**, in both toluene and CH_2Cl_2, illustrates on the one hand the influence of the substituent at the C-2 atom of the heterocyclic ring and, on the other, the effect played by the solvent on the steric course (Fig. 2).

In every case the reaction pathways leading to **10** and **19** involve two steps with analogous stationary points (black lines in Fig. 2). On the other hand, the alternative approaches, similar to each other as well, leading to regioisomers **20** and **21** take place through a single transition structure (red lines in Fig. 2). At first glance, concerted pathways are disfavored with respect to stepwise cycloadditions, pointing to a regiospecific course that is consistent with our experimental results. Remarkably, reactions of **1** and **7** in both solvents are characterized by flat free energy profiles in the vicinity of transition structures [e.g., $\Delta\Delta G$(**TS2$_{19}$t-TS1$_{19}$t**) = 0.79 kcal mol^{-1} and $\Delta\Delta G$(**TS2$_{19}$t-I$_{19}$t**) = 1.79 kcal mol^{-1}], with formation of the second C–C bond as the rate-determining step (Fig. 2A and B).

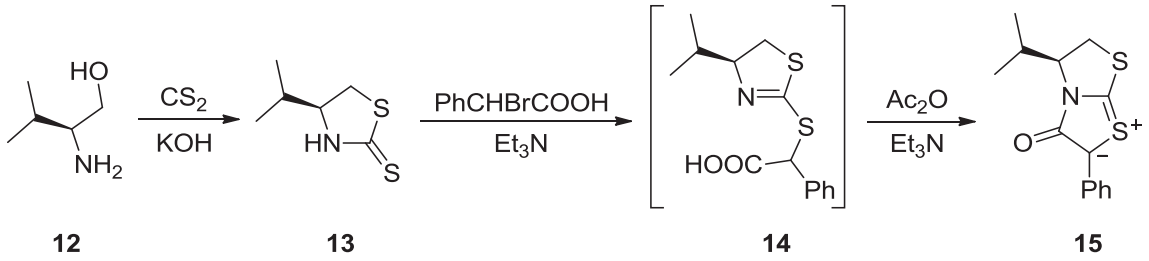

Scheme 2. Preparation of chiral thioisomünchnone **15**.

Reactions of **3** and **7**, irrespective of the solvent too, show higher differences in their energy barriers [e.g., $\Delta\Delta G$(**TS1$_{10}$t-TS2$_{10}$t**) = 4.03 kcal mol^{-1} and $\Delta\Delta G$(**TS1$_{10}$t-I$_{10}$t**) = 6.88 kcal mol^{-1}], being now the rate-determining step the first C–C bond-forming reaction (Fig. 2C and D). Moreover, compound **3** reacts with **7** faster than **1** in both solvents [$\Delta\Delta G$(**TS2$_{19}$t-TS1$_{10}$t**) = 2.85 kcal mol^{-1} and $\Delta\Delta G$(**TS2$_{19}$d-TS1$_{10}$d**) = 2.25 kcal mol^{-1}]. These results demonstrate the influence exerted by a substituent other than hydrogen as well as solvent effects on the reactivity of thioisomünchnones and, they also agree with the higher stabilization of polar zwitterionic intermediates in CH_2Cl_2 [$\Delta\Delta G$(**I$_{19}$t-I$_{19}$d**) = 1.28 kcal mol^{-1} and $\Delta\Delta G$(**I$_{10}$t** − **I$_{10}$d**) = 2.41 kcal mol^{-1}]. Table 1 shows the energy gaps ($\Delta\Delta E$, $\Delta\Delta H$, and $\Delta\Delta G$) that separate the first saddle points of the stepwise cycloadditions from the corresponding zwitterionic intermediates, determined in both toluene and CH_2Cl_2.

Inspection of $\Delta\Delta E$, $\Delta\Delta H$ and $\Delta\Delta G$ values indicates that the stabilization of **I$_{10}$** is greater than that of **I$_{19}$** with respect to transition structures **TS1$_{10}$** and **TS1$_{19}$** in either solvent. These results show that the phenyl group linked to C-2 at the mesoionic heterocycle destabilizes the intermediate, especially as the solvent polarity increases. The major stability of **I$_{10}$** with respect to **I$_{19}$** is somewhat mirrored by the second transition structures (**TS2$_{10}$** and **TS2$_{19}$**), given the close similarity in both structure and energy between those saddle points and the corresponding zwitterionic intermediates [$\Delta\Delta G$(**TS2$_{19}$t-TS2$_{10}$t**) = 6.88 kcal mol-1 and $\Delta\Delta G$(**TS2$_{19}$d-TS2$_{10}$d**) = 7.16 kcal mol-1].

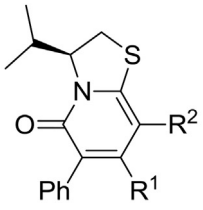

16 $R^1 = R^2 =$ COOMe
17 $R^1 =$ H, $R^2 =$ COOMe
18 $R^1 =$ H, $R^2 =$ COOEt

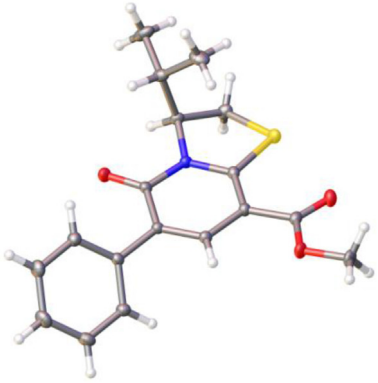

Fig. 1. Solid-state structure of compound **17**. Crystal data were collected at 100(2) K; orthorhombic crystal system ($P2_12_12_1$ space group); ellipsoids drawn at 50% probability.

In order to understand the greater reactivity of **3** in the above cycloaddition, we performed a NSA (*natural steric analysis*)[13] for the approaches of **7** to **1** and **3** in toluene and CH_2Cl_2, which expresses the steric exchange repulsion as the energy difference due to NLMO (*natural localized molecular orbital*) orbital orthogonalization.[14] Table 2 shows the results obtained by comparing the total dE(i) for each TS (**TS1$_{19}$t**, **TS1$_{10}$t**, **TS1$_{19}$d**, and **TS1$_{10}$d**) with the total dE(i) values calculated when both dipolarophile and dipole fragments (**7** against dipoles **1** and **3**) are separated by a large distance (12.0 Å), in order to ensure both partners do not interact with each other.

The intermolecular dE(i) values associated to the approach of **7** and **1** are higher than that of **7** with **3** (36.66 kcal mol^{-1} in toluene and 19.37 kcal mol^{-1} in CH_2Cl_2). However, as expected, the intermolecular dE(i) values are very similar for the regioisomeric concerted processes.

Concerted *vs* Stepwise Processes. The intermolecular steric exchange [$\Delta dE(i)_{total}$] is disfavored for the concerted cycloadditions (**TS1$_{10}$t-TS$_{21}$t** = −31.66 kcal mol^{-1}, **TS1$_{19}$d-TS$_{20}$d** = −19.93 kcal mol^{-1}, and **TS1$_{10}$d-TS$_{21}$d** = −43.80 kcal mol^{-1}) with the exception of **TS1$_{19}$t-TS$_{20}$t** (8.18 kcal mol^{-1}), thus suggesting that in this case the intermolecular steric repulsion is not responsible for a preferential stepwise process (*vide infra*).

Although structures **TS1$_{19}$t** and **TS1$_{19}$d** are quite similar, their $dE(i)_{total}$ values differ by 34.14 kcal mol^{-1}. In order to justify this energy difference we compared the NLMO contributions to the total steric exchanges for saddle points **TS1$_{19}$t** and **TS1$_{19}$d**. Results show a very similar orbital distribution and energy contributions, although for **TS1$_{19}$t** the LP_{C8} (for the sake of clarity, numbering is shown in Fig. 3) contributes significantly (26.60 kcal mol^{-1}) to $dE(i)_{total}$, thus destabilizing the system. The major portion of this contribution corresponds to the interactions of LP_{C8}-$\sigma_{C5\text{-}C6}$ and LP_{C8}-$\sigma_{C6\text{-}S9}$ NLMO pairs (Fig. 4).

As collected in Table 3, the stabilization by charge transfer (CT) is always higher for the stepwise processes, especially for the reaction of **1** and **7** in toluene (521.46 kcal mol^{-1}). The highest total CT for **TS1$_{19}$t** (1847 kcal mol^{-1}) should be attributed to the methyl propiolate contribution (749.32 kcal mol^{-1}). **TS1$_{19}$t** and **TS1$_{19}$d** exhibit very similar NBO (*natural bond orbital*)[15] distribution and energy contribution to CT, though the CT of the NBO LP_{C8} stabilizes the system by 305.98 kcal mol^{-1}. In fact the highest CT value for **TS1$_{19}$t** corresponds to transfer from LP_{C8} to $\pi^*_{C20\text{-}O21}$ (170.19 kcal mol^{-1}) (Fig. 5). The greater stabilization of **TS1$_{19}$t** provided by charge transfer would then account for a favorable process leading to **19**

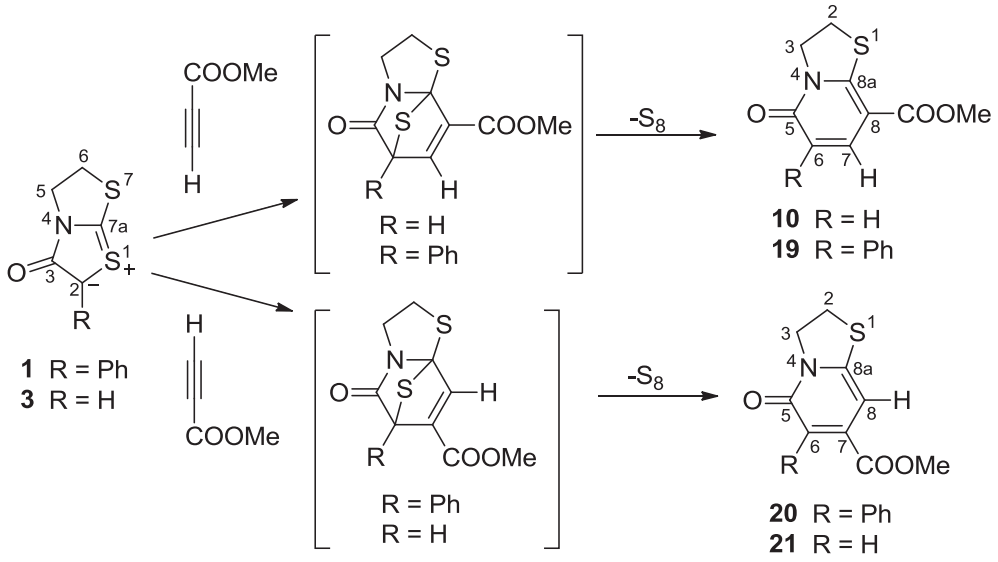

Scheme 3. Regiochemical approaches of methyl propiolate (**7**) to mesoionic **1** and **3**.

with respect to the concerted pathway, thereby offsetting the intramolecular steric exchange exerted by the dipolarophile.

The CTs from dipole to dipolarophile are greater in the saddle points of stepwise processes than those of concerted pathways. For **TS1$_{19}$t** the highest contribution corresponds to the interaction of LP_{C6} with LV_{C7} and $RY(1)_{C7}$ (23.92 and 95.45 kcal mol^{-1}, respectively). In the case of **TS1$_{19}$d** the CT goes from LP_{C6} to $\pi(2)^*_{C7\text{-}C8}$ (128.29 kcal mol^{-1}) (Fig. 6).

For the cycloaddition of thioisomünchnone **3**, the greater contributions to CT in **TS1$_{10}$t** correspond to the interaction of $\pi_{C6\text{-}S9}$ and $\pi^*_{C6\text{-}S9}$ to $\pi(2)^*_{C7\text{-}C8}$ (13.03 and 98.66 kcal mol^{-1} respectively). Finally, the NBOs of **TS1$_{10}$d** are identical to those of **TS1$_{10}$t**, though with slightly lower energy values (12.40 and 90.77 kcal mol^{-1}, respectively) (Fig. 7).

In **TS1$_{19}$t** and **TS1$_{19}$d** the major contribution involved in CT arises from the donor NBO LP_{C6}, while for **TS1$_{10}$t** and **TS1$_{10}$d** there is an important contribution from the $\pi_{C6\text{-}S9}$ orbital. Such a difference can be attributed to electron delocalization of LP_{C6} with the phenyl group in **TS1$_{19}$t** and **TS1$_{19}$d**, absent in **TS1$_{10}$t** and **TS1$_{10}$d**, for which the charge is instead delocalized with the sulfur atom. The acceptor NBO for **TS1$_{19}$d**, **TS1$_{10}$t**, and **TS1$_{10}$d** is the $\pi(2)^*_{C7\text{-}C8}$ orbital, whereas for **TS1$_{19}$t** the acceptor role is played by the empty NBOs at C7. The lack of $\pi(2)_{C7\text{-}C8}$ and $\pi(2)^*_{C7\text{-}C8}$ orbitals in **TS1$_{19}$t** could be ascribed to the high electron delocalization of LP_{C8} with the methoxycarbonyl group (Fig. 5).

For the opposite regiochemistry, the CT from the dipolarophile to the dipole is greater than in the reverse direction. For all transition structures (**TS$_{20}$t**, **TS$_{20}$d**, **TS$_{21}$t** and **TS$_{21}$d**) the main contribution to CT goes from the $\pi 2_{C7\text{-}C8}$ to $\pi^*_{C8a\text{-}N4}$ (65.66, 69.94, 44.25, and 47.96 kcal mol^{-1}, respectively) (Fig. 8). All in all, these results would justify the prevalent approach of the C6-C7 bond to the C8a-C7 fragment.

2.3. Facial stereoselection

Taking into account the chiral nature of thioisomünchnone **15**, its cycloaddition with **6** could take place by any of the two faces of the heterocycle to give the initial cycloadducts **22** and **23**. In the case of unsymmetrically-substituted alkynes such as **7** and **8**, the corresponding approaches could also occur through two different orientations, leading to cycloadducts **24**–**27** and **28**–**31**, respectively.

Fig. 9 shows the energetic profiles for the four possible reaction channels involving the cycloaddition of thioisomünchnone **15** with **7** in toluene. Again, the regiochemistry is related to the concerted or non-concerted nature of the process, and the calculated energy barriers (Fig. 9A) are quite similar to those previously found for the reaction of **1** and **7** (Fig. 2A), which clearly reflects the close structural similarity of thioisomünchnones **1** and **15**.

The stepwise cycloadditions leading to thiazolopyridone **17** constitute the most favored reactions. When the dipolarophile attacks to the *Re*-2,*Re*-7a face of **15**, namely the opposite face to the isopropyl group (Fig. 9A), the energy barrier is 5.46 kcal mol^{-1} lower than that for a concerted mechanism (red line), thereby pointing to the sole formation of cycloadduct **24**. The same happens when **7** approaches to **15** through the *Si*-2,*Si*-7a face [$\Delta\Delta G^{\ddagger}$(**TS$_{27}$**–**TS1$_{25}$**) = 4.99 kcal mol^{-1}] giving rise to cycloadduct **25**. Both cycloadducts (**24** and **25**) evolve to the same thiazolopyridone (**17**) after sulfur extrusion. Surprisingly, the interaction of **7** with the *Si*-2,*Si*-7a face of **15** (**TS1$_{25}$**) is kinetically favored (Fig. 9B) with respect to **TS1$_{24}$** (by 1.41 kcal mol^{-1} only), a fact consistent with the poor facial stereoselection exhibited by thioisomünchnone **15**. The lack of stereoselection could also be interpreted in geometric terms, i.e. compound **7** is rather linear-shaped and lies far to the stereodiscriminating isopropyl group in **TS1$_{25}$**.

In following the same methodology reported above, we performed an NSA[13] intermolecular study for both approaches of **7** to **15** (**TS1$_{24}$** and **TS1$_{25}$**). Results are given in Table 4.

The dE(i) values obtained for saddle points **TS1$_{24}$** and **TS1$_{25}$** indicate that the intermolecular steric exchange between the dipole and its dipolarophile is 9.22 kcal mol^{-1} lower when **7** approaches to **15** at the *Si*-2,*Si*-7a face, which contains the bulky isopropyl group, than the addition at the rear face.

In order to understand the origin of these results, we performed a *natural bond critical point analysis* (NBCP).[16] The CPs are points where the gradient of the electronic density, [$\nabla\rho(\mathbf{r})$], is zero, and they are characterized by three eigenvalues (λ_1, λ_2, λ_3) of the Hessian matrix of $\rho(\mathbf{r})$. The CPs are identified as (*r*,*s*) according with their rank (number of nonzero eigenvalues) and signature (algebraic sum of eigenvalues signs). A (3,-1) CP in which $\rho(\mathbf{r})$ diminishes in two directions and increases in the third, is a saddle point of $\rho(\mathbf{r})$ found between two neighboring atoms and it defines the linkage between them (BCP). When the Laplacian of $\rho(\mathbf{r})$ [$\nabla^2\rho(\mathbf{r})$], namely the sum of three eigenvalues (λ_1, λ_2, λ_3), is negative the electronic

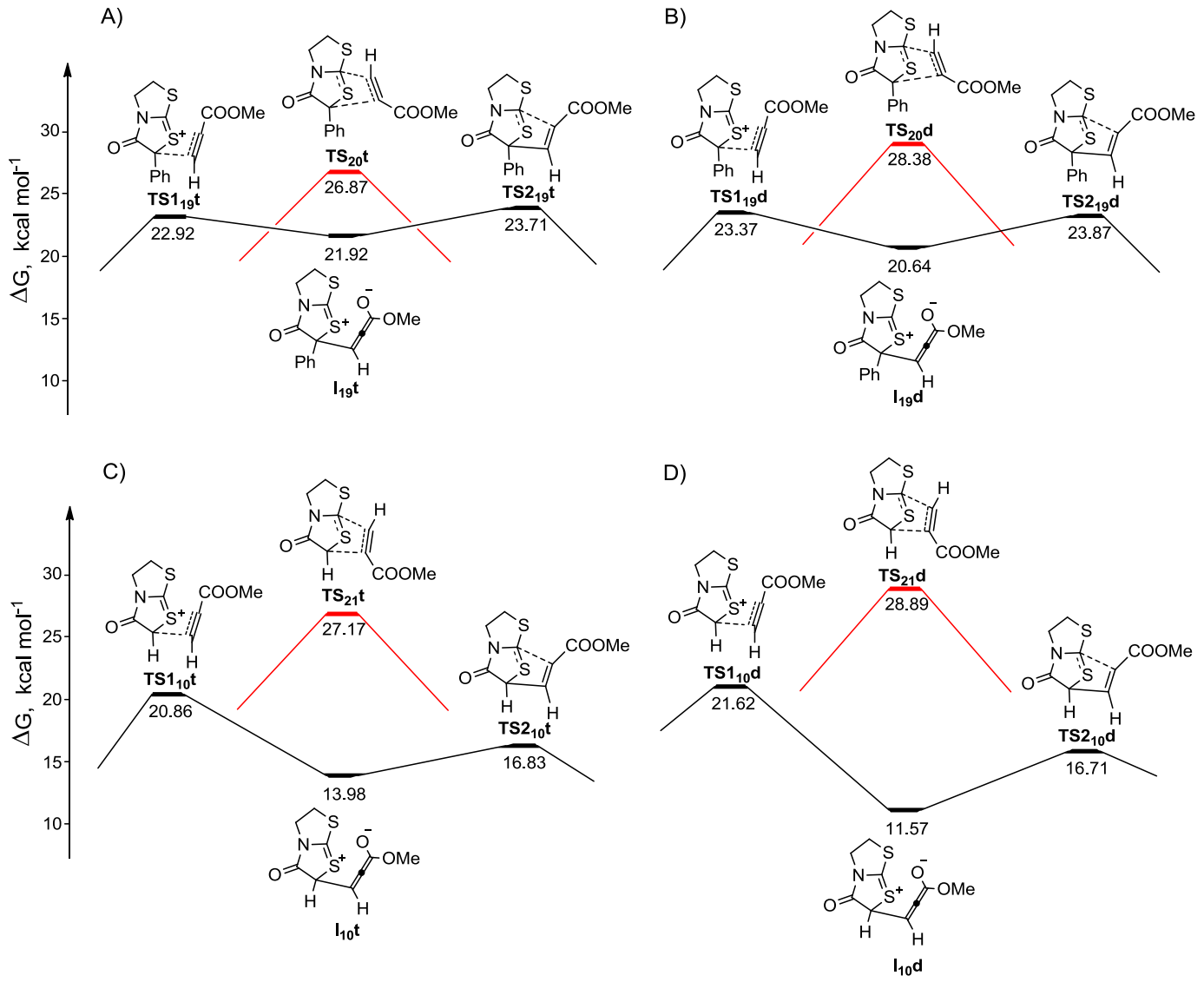

Fig. 2. Relative free energy barriers (kcal mol^{-1}) for transition structures and intermediates involved in the 1,3-dipolar cycloadditions of **1** (A and B) and **3** (C and D) with methyl propiolate (**7**) in toluene (A and C) and CH_2Cl_2 (B and D). Black lines describe the more favored route whereas the regioisomeric pathways are depicted in red.

charge is concentrated within the region of the BCP which is characteristic of covalent or polarized bonds, namely a shared layer interaction. However, a positive $\nabla^2\rho(\mathbf{r})$ corresponds to a charge leakage area, characteristic of a closed shell interaction. In the transition structure **TS1$_{25}$** the calculated distance between the carbonyl oxygen of **7** (O21 in Fig. 5) and the nearest methyl hydrogen of **15** (H11 in Fig. 10) is 2.60 Å, and the eigenvalues of the Hessian matrix are $\lambda_1 = 0.0403$, $\lambda_2 = -0.0067$, and $\lambda_3 = -0.0068$. Accordingly, this CP is identified to be a first-order saddle point [(3,-1)]. The magnitudes of $\rho(\mathbf{r})$ and $\nabla^2\rho(\mathbf{r})$ for the aforementioned CP are quite small (0.0085 and 0.0268 au, respectively), pointing a weak interaction, and the positive value of $\nabla^2\rho(\mathbf{r})$ suggests a closed

Table 1
Electronic energy, enthalpy, and free energy gaps between the first saddle point and the corresponding intermediate (in kcal mol^{-1}) for cycloadditions of **1** and **3** with **7**, in toluene and CH_2Cl_2.

Structure	ΔE[a]	ΔH[a]	ΔG[a]	$\Delta\Delta E$	$\Delta\Delta H$	$\Delta\Delta G$
TS1$_{19}$t	9.16	9.76	22.92	3.84	2.74	1.00
I$_{19}$t	5.32	7.02	21.92			
TS1$_{19}$d	10.40	10.70	23.37	6.38	5.02	2.73
I$_{19}$d	4.02	5.68	20.64			
TS1$_{10}$t	6.68	7.32	20.86	9.05	7.59	6.88
I$_{10t}$	−2.37	−0.27	13.98			
TS1$_{10}$d	7.63	8.23	21.62	11.73	10.21	10.05
I$_{10}$d	−4.10	−1.98	11.57			

[a] Relative to reagents.

Table 2
Occupied NLMO contributions [dE(i), kcal mol^{-1}] to intermolecular steric exchange energy in transition structures **TS1$_{19}$t**, **TS1$_{10}$t**, **TS1$_{19}$d**, **TS1$_{10}$d**, and **TS$_{20}$t**, **TS$_{21}$t**, **TS$_{20}$d**, **TS$_{21}$d**.

Structure	dE(i)$_{total}$	dE(i)$_{total\ at\ 12.0\ Å}$	ΔdE(i)$_{total}$	$\Delta\Delta$dE(i)$_{total}$
TS1$_{19}$t	1419.89	1256.68	163.21	36.66
TS1$_{10}$t	846.56	720.01	126.55	
TS1$_{19}$d	1385.75	1249.65	136.10	19.37
TS1$_{10}$d	837.54	720.81	116.73	
TS$_{20}$t	1448.39	1293.36	155.03	−3.18
TS$_{21}$t	903.14	744.93	158.21	
TS$_{20}$d	1444.53	1288.50	156.03	−4.50
TS$_{21}$d	904.54	744.01	160.53	

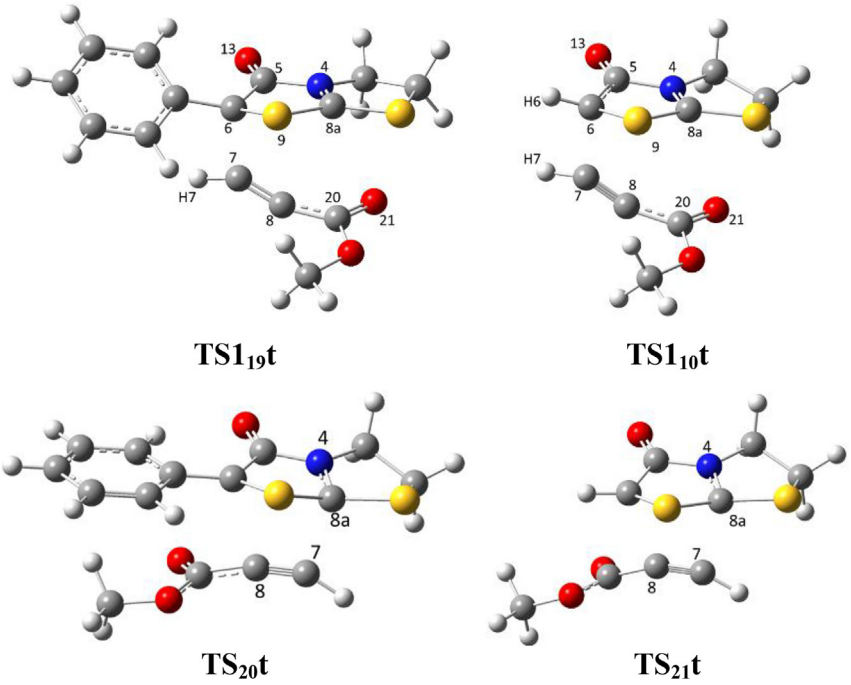

Fig. 3. M06-2X/6−311++G(d,p)-optimized structures of **TS1$_{10}$t**, **TS1$_{19}$t**, **TS$_{20}$t**, and **TS$_{21}$t** in toluene (SMD method).

shell interaction. The NLMO contributions to $\rho(\mathbf{r})$ and $\nabla^2\rho(\mathbf{r})$ for this BCP are shown in Table 5.

The correlation (in percentage) of such NLMOs with their parent localized NBOs is extremely high, all over 98.8%, which points to a high electron localization at these NLMOs. The charge transfer (CT) energy between these NBOs goes from the first lone pair of the O21 atom to the $\sigma^*_{C11\text{-}H11}$ orbital (0.21 kcal mol^{-1}) and from the second pair of the same oxygen atom to the $\sigma^*_{C11\text{-}H11}$ and $\sigma^*_{C11\text{-}H11'}$ orbitals (0.34 and 0.10 kcal mol^{-1}, respectively). Overall, these interactions stabilize the system and their total value (0.65 kcal mol^{-1}) can be interpreted in terms of a weak van der Waals interaction.

Table 6 shows the steric interactions of occupied NLMOs of methyl propiolate (**7**) with the isopropyl group of **15** in **TS1$_{25}$**. Again these steric interactions are very small [$\Sigma dE(i,j) = 3.61$ kcal mol^{-1}], thus proving that the isopropyl group does not destabilize the system by steric repulsions, at least to an appreciable extent. Since this alkyl group does not appear to be responsible for the greater stability of **TS1$_{25}$**, we then considered the saddle point moiety in which both transition structures (**TS1$_{24}$** and **TS1$_{25}$**) match, namely formation of the C6-C7 bond (Table 7).

Both BCPs$_{C6\text{-}C7}$ in **TS1$_{24}$** and **TS1$_{25}$** are very similar with small values for $\rho(\mathbf{r})$ and $\nabla^2\rho(\mathbf{r})$. However $\nabla^2\rho(\mathbf{r})$ is positive for **TS1$_{24}$**, and therefore indicative of a closed shell interaction, while it is negative for **TS1$_{25}$**, which corresponds to a shared layer interaction. Table 8 shows the NLMO contributions to $\rho(\mathbf{r})$ and $\nabla^2\rho(\mathbf{r})$ for these BCPs.

Clearly, in both TSs the largest contributor to $\rho(\mathbf{r})$ in such BCPs is the LP$_{C6}$ orbital, and the corresponding $\nabla^2\rho(\mathbf{r})$ values suggest that the electron densities are highly localized in those NLMOs; or in other words, they reflect the nucleophilic character of the carbon atom in question, which is slightly higher in **TS1$_{25}$**. The low correlation percentage of these NLMOs with their parent localized NBOs (57.86% for **TS1$_{24}$** and 57.33% for **TS1$_{25}$**) suggests a significant level of electron delocalization, which in turn justifies a high charge transfer (CT) efficiency between these NBOs and the closer empty NBOs (see Table S4).

The total stabilization energy by CT ascribed to the lone pair that initiates the nucleophilic attack is higher for **TS1$_{25}$** than that for **TS1$_{24}$** (33.10 kcal mol^{-1}). The delocalization between the heterocycle and the alkyne reagent is quite similar for both saddle points (only 4.76 kcal mol^{-1} higher in energy for **TS1$_{24}$**), albeit electron delocalization of the LP$_{C6}$ orbital with the phenyl group is higher in **TS1$_{25}$** (31.04 kcal mol^{-1}) than in **TS1$_{24}$** (1.53 kcal mol^{-1}). Likewise, electron delocalization of LP$_{C6}$ with the Rydberg orbitals of C6, C5, S9, and C14 is somewhat higher in **TS1$_{25}$** (21.85 kcal mol^{-1}) than in **TS1$_{24}$** (13.19 kcal mol^{-1}). Together these data account for a preferential cycloaddition of **7** to **15** on the *Si*-2,*Si*-7a face of the latter (**TS1$_{25}$**).

Table 3 showed that for **TS1$_{19}$t** a high charge transfer takes place in the dipolarophile fragment (749.32 kcal mol^{-1}). For **TS1$_{24}$** and **TS1$_{25}$** these values are quite similar (735.03 and 799.72 kcal mol^{-1}). In fact, the most important contribution to CT is given by the interaction of LP$_{C8}$ to $\pi^*_{C20\text{-}O21}$ with energy values of 157.91 and 190.07 kcal mol^{-1} for **TS1$_{24}$** and **TS1$_{25}$**, respectively, exactly the same as for **TS1$_{19}$t**. Also, Table S4 shows the CT from the donor NBO LP$_{C6}$ to LV$_{C7}$ and RY(1)$_{C7}$ for **TS1$_{24}$** and **TS1$_{25}$**. In such interactions the orbital participation is identical to those shown in Fig. 6A and B for **TS1$_{19}$t**, and the corresponding CT values are quite similar as well. In short, transition structure **TS1$_{19}$t** has the same orbital distribution and almost identical energy values as those of **TS1$_{24}$** and **TS1$_{25}$**, all of them optimized in toluene.

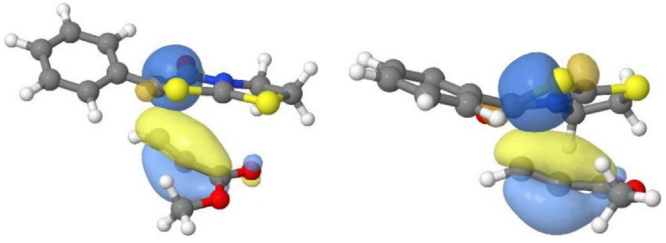

Fig. 4. Main contributions of the NLMO LP$_{C8}$ to steric repulsion in **TS1$_{19}$t**. Left: LP$_{C8}$-$\sigma_{C5\text{-}C6}$ interaction; right: LP$_{C8}$-$\sigma_{C6\text{-}S9}$ interaction.

Table 3
Different charge transfer (kcal mol^{-1}) contributions from occupied to empty NBOs for transition structures **TS1t**, **TS1d**, **TSt** and **TSd**.

Structure	Within dipole	From dipole to dipolarophile	From dipolarophile to dipole	Within dipolarophile	Total CT	ΔCT
TS1$_{19}$t	930.62	147.8	19.95	749.32	1847.69	521.46
TS$_{20}$t	867.03	57.39	96.34	305.47	1326.23	
TS1$_{19}$d	945.64	163.11	15.18	306.51	1430.44	96.37
TS$_{20}$d	867.70	59.52	102.30	304.55	1334.07	
TS1$_{10}$t	569.23	140.94	12.2	311.56	1033.93	143.72
TS$_{21}$t	460.48	67.02	66.04	296.67	890.21	
TS1$_{10}$d	578.39	130.82	11.06	308.92	1029.19	126.64
TS$_{21}$d	464.31	69.93	70.44	297.87	902.55	

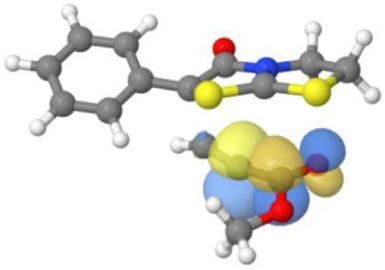

Fig. 5. Highest CT in **TS1$_{19}$t** from NBO LP$_{C8}$ to $\pi^*_{C20\text{-}O21}$.

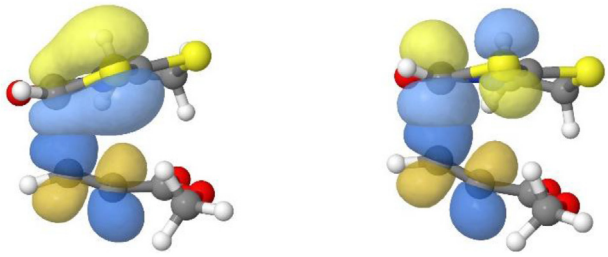

Fig. 7. Charge transfers from NBO $\pi_{C6\text{-}S9}$ (left) and $\pi^*_{C6\text{-}S9}$ (right) to $\pi(2)^*_{C7\text{-}C8}$ in **TS1$_{10}$d**.

3. Conclusions

Two structurally rigid thioisomünchnone dipoles (**3** and **15**) have been prepared by condensation of α-haloacids with thiazolidin-2-thiones (**4** and **13**) under basic conditions. The mesoionic dipole **3** was generated *in situ* and then trapped with acetylenes, thus providing a one-pot route to novel 8-alkoxycarbonyl-5-oxo-3,5-dihydro-2*H*-thiazolo[3,2-*a*]pyridines (**9**–**11**). The structural characterization of products derived from asymmetrically-substituted dipolarophiles could be successfully accomplished through NMR spectroscopy due to the vicinal disposition of hydrogen atoms at C-6 and C-7 of the heterocycles. Cycloadditions conducted with chiral thioisomünchnone **15** afforded optically active products, namely (*S*)-3-isopropyl-5-oxo-6-phenyl-3,5-dihydro-2*H*-thiazolo[3,2-*a*]pyridines **16**–**18**, whose structural characterization could be achieved by comparing their spectroscopic data to those of **17**, the latter being unequivocally elucidated by single-crystal X-ray diffraction. In all cases, the use of asymmetrically-substituted dipolarophiles proceeded with complete regioselectivity.

The experimental results have been corroborated by a detailed DFT study, at the M062-X/6-311++G(d,p) level of theory, with inclusion of solvents effects (through the SMD model) in toluene and CH_2Cl_2. All cycloadditions involving methyl propiolate (**7**) giving rise to the regioisomer isolated experimentally are stepwise processes, while an opposite orientation of the dipolarophile turned out to be a concerted mechanism. Data collected in Fig. 2 show that a phenyl group at C-2 of the mesoionic dipole lead to higher energy barriers for these cycloadditions. All concerted transformations are disfavored, a fact that can be rationalized in terms of intermolecular steric repulsions during the dipole-dipolarophile interaction, which are indeed greater for all concerted pathways with the sole exception of **TS1$_{19}$t**. This behavior is well counterbalanced by a large stabilization due to charge transfer in **TS1$_{19}$t** of the LP$_{C8}$ (in the dipolarophile's fragment), thereby accounting for a stepwise pathway too. Moreover, this behavior for **TS1$_{19}$t** can also be inferred from a comparative analysis with transition structures **TS1$_{24}$** and **TS1$_{25}$**, which have also been optimized in toluene and exhibit an almost identical orbital distribution to **TS1$_{19}$t**.

It is known that most common 1,3-dipolar cycloadditions can be interpreted as Sustmann type I processes involving a nucleophilic attack from the dipole to the dipolarophile. This kind of cycloadditions is consistent with stepwise cycloadditions studied herein, for which the nucleophilic addition involves the C-6 atom of the dipole and the C-7 atom of the dipolarophile. Data gathered for the opposite orientation of **7** suggest that the nucleophilic attack goes from C-7 of the dipolarophile to C-8a of the dipole, thus becoming a Sustmann type III cycloaddition. The saddle points **TS1$_{24}$** and **TS1$_{25}$** correspond to the approach of **7** to both faces of chiral thioisomünchnone **15**. Subsequent comparative analyses of intermolecular steric repulsions for the above TSs have ultimately proven that the isopropyl group does not exert a marked steric repulsions; in fact there is actually a minor stabilization by charge transfer.

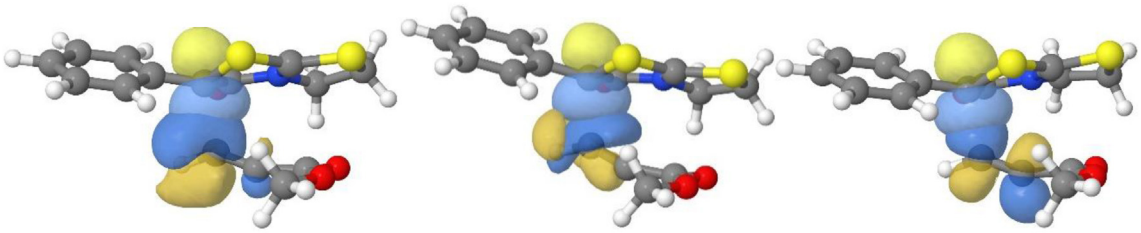

Fig. 6. NBOs CT from LP$_{C6}$ to LV$_{C7}$ (A) and RY(1)$_{C7}$ (B) in **TS1$_{19}$t**, and to $\pi(2)^*_{C7\text{-}C8}$ (C) in **TS1$_{19}$d**.

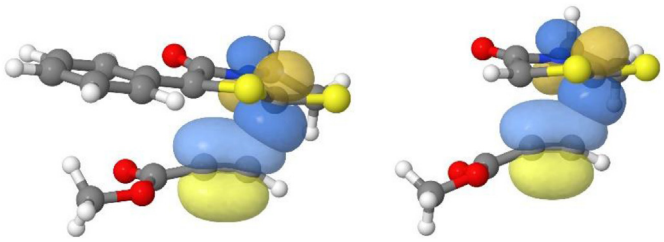

Fig. 8. Charge transfers from NBO $\pi 2_{C7\text{-}C8}$ to $\pi^*_{C8a\text{-}N4}$ in **TS$_{20}$t** and **TS$_{21}$t**.

4. Experimental section

4.1. General methods

Solvents and reagents were purchased from commercial suppliers and used without further purification. The identity of all compounds was confirmed by their elemental analysis, high-resolution mass spectra, mps, and NMR data (see SI).

4.2. Computational details

All calculations reported in this work were carried out using the Gaussian09 package.[17] The M06-2X[18] density functional method in conjunction with the 6-311++G(d,p)[19] basis set were selected for all the geometry optimizations and frequency analysis. The geometries were optimized including solvation effects in toluene and CH_2Cl_2, which have been determined by the density-based self-consistent reaction field theory of bulk electrostatic, i.e., the well-known solvation model density (SMD)[20] method that takes into account different contributions such as long-range electrostatic polarization (bulk solvent effect). Frequency calculations at 298.15 K on all the stationary points were carried out at the same level of theory as the geometry optimizations to ascertain the nature of the stationary points. Ground and transition states were characterized by none and one imaginary frequency, respectively. NSA (*natural steric analysis*),[13] which evaluates the occupied NLMO contributions [dE(i)], NBCP (*natural bond critical point analysis*)[16] and CT (*charge transfer*) analysis were all carried out with the NBO 6.0 package.[21] Main orbital [NBO[15] (*natural bond orbital*) and NLMO[14] (*natural localized molecular orbital*)] interactions have been represented with the Jmol software.[22] All of the relative energies shown are free energies calculated at 298.15 K with respect to the reagents.

Table 4
Occupied NLMO contributions [dE(i) in kcal mol^{-1}] to the intermolecular steric exchange energy for transition structures **TS1$_{24}$** and **TS1$_{25}$** in toluene.

Structure	$dE(i)_{total}$	$dE(i)_{total}$ at 12.0 Å	$dE(i)_{total}$ - $dE(i)_{total}$ at 12.0 Å
TS1$_{24}$	1647.12	1504.13	142.99
TS1$_{25}$	1650.30	1516.53	133.77

4.2.1. 2-((4,5-Dihydrothiazol-2-yl)thio)acetic acid (**5**)

To a solution of thiazolidine-2-thione (**4**) (8.4 mmol) in CH_2Cl_2 and bromoacetic acid (8.4 mmol) was added triethylamine and the mixture was stirred a room temperature for 72 h. Then, the resulting triethylammonium bromide was filtered off. In order to remove dissolved salts the, the solution was also passed through a silica gel [Merck 60 (400-230 mesh)] column using ethyl acetate as eluent. The solvent was evaporated to dryness to give a white solid (91%). Mp 125–126 °C. FTIR (KBr) ν_{max} 3002, 2957, 2786, 2365, 1885, 1710, 1557, 1388, 1317, 1186, 1036, 895, 678, 656, 447 cm^{-1}. ^{1}H NMR (500 MHz, $CDCl_3$, 25 °C) δ 4.25 (t, 2H, J = 8.0 Hz), 3.71 (s, 2H), 3.56 (t, 2H, J = 8.0 Hz) ppm. ^{13}C NMR (125 MHz, $CDCl_3$, 25 °C) δ 173.6, 169.1, 61.8, 36.5, 35.4 ppm. Anal. Calcd for $C_5H_7NO_2S_2$: C, 33.90; H, 3.95; N, 7.91; S, 36.16. Found: C, 34.11; H, 4.12; N, 7.83; S, 36.26.

4.2.2. (S)-5-Isopropyl-2-phenyl-5,6-dihydrothiazolo[2,3-b]thiazol-4-ium-3-olate (**15**)

A mixture of (*S*)-4-isopropylthiazolidine-2-thione (**13**) (23 mmol), 2-bromo-2-phenylacetic acid (23 mmol), and triethylamine (23 mmol) in benzene (50 mL) was stirred at room temperature for 72 h. The resulting precipitate of triethylammonium bromide was filtered off. To remove dissolved salts the solution was also passed through a silica gel [Merck 60 (400-230 mesh)] column using ethyl acetate as eluent. The solvent was evaporated to dryness to give an oily residue (5.4 g), which contained the intermediate thioglycolic acid **14**. To this oil a mixture of triethylamine an acetic anhydride (3:1, 40 mL) was added. The mixture was softly heated for a few minutes, yielding the title compound as orange crystals which were collected by filtration and washed with diethyl ether (50%). Mp 190–192 °C. [α]$_D$ 177.8° (c 5.1, CH_2Cl_2). FTIR (KBr) ν_{max}. 3052, 3023, 2961, 2917, 2864, 1645, 1504, 1495, 1443, 1189, 754, 697, 687 cm^{-1}.

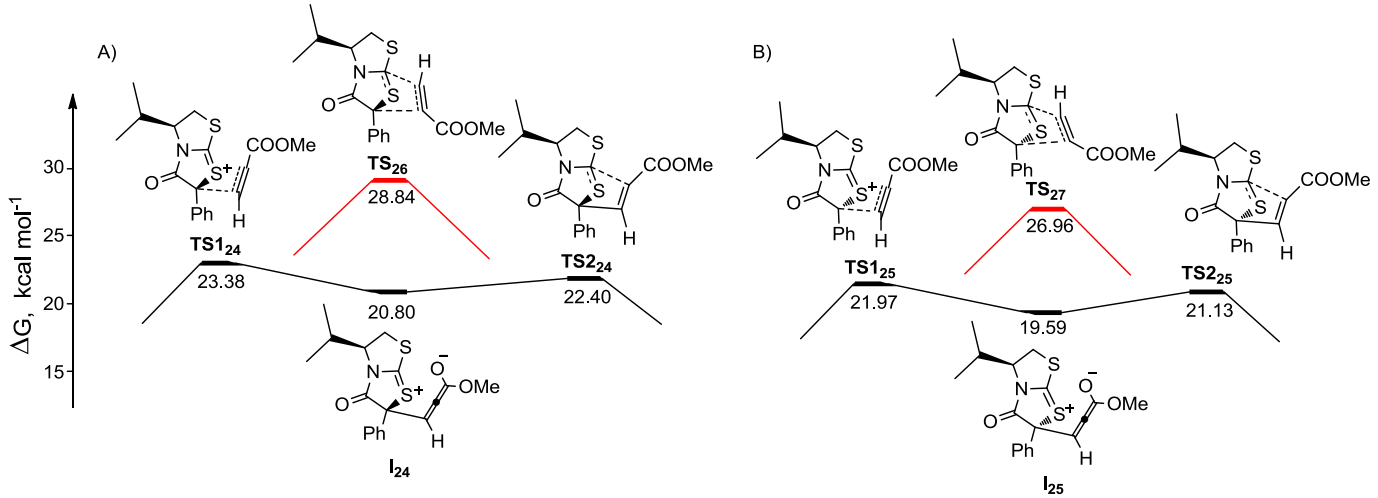

Fig. 9. Relative free energy barriers (kcal mol^{-1}) for transition structures and intermediates involved in the regioselective approaches of **7** to the *Re*-2,*Re*-7a (Figure A) and *Si*-2,*Si*-7a (Figure B) faces of **15** in toluene. In every case, black lines denote the more favored route whereas the regioisomeric pathways are depicted in red.

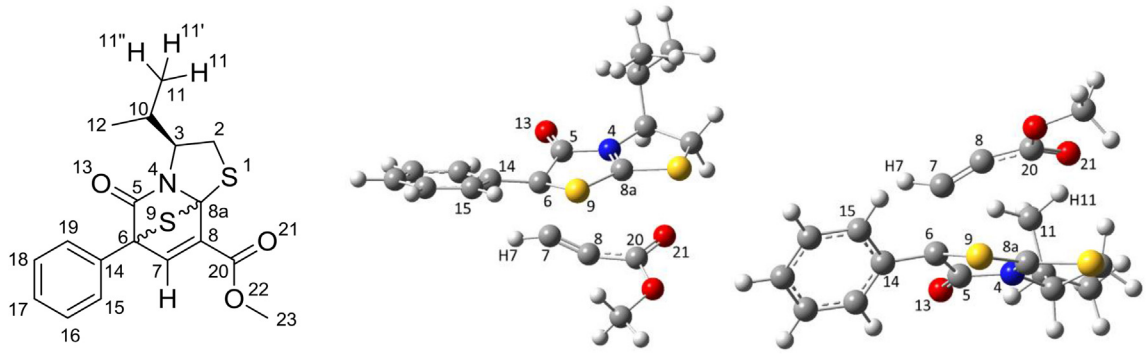

Fig. 10. M06-2X/6-311++G(d,p)-optimized structures of **TS1$_{24}$** and **TS$_{25}$** in toluene (SMD method).

Table 5
NLMO contributions to ρ(**r**) and $\nabla^2\rho(\mathbf{r})$ for the BCP$_{O21\text{-}H11}$ in **TS1$_{25}$**.

NLMO	% ρ(r)	$\nabla^2\rho$(r) (au)
LP(1)$_{O21}$	15.90%	0.0058
LP(2)$_{O21}$	33.50%	0.0061
$\sigma_{C11\text{-}H11}$	45.50%	0.0125
$\sigma_{C11\text{-}H11'}$	2.80%	0.0004

Table 6
Steric exchange energies (in kcal mol^{-1}) for i,j NLMOs of **7** with the isopropyl group of **15** in **TS1$_{25}$**.

NLMO(i)	NLMO(j)	dE(i,j)
LP(1)$_{O21}$	$\sigma_{C11\text{-}H11}$	0.42
	$\sigma_{C11\text{-}H11'}$	0.05
LP(2)$_{O21}$	$\sigma_{C11\text{-}H11}$	0.09
	$\sigma_{C11\text{-}H11'}$	0.80
	$\sigma_{C11\text{-}H11''}$	0.08
$\pi_{C7\text{-}C8}$	$\sigma_{C11\text{-}H11}$	2.04
	$\sigma_{C11\text{-}H11'}$	0.07
	$\sigma_{C11\text{-}H11''}$	0.06
		ΣdE(i,j) = 3.61

^{1}H NMR (500 MHz, $CDCl_3$, 25 °C) δ 7.74 (dd, 2H, J = 1.0 Hz, J = 8.5 Hz), 7.29 (dd, 2H, J = 7.5 Hz, J = 8.0 Hz), 7.05 (m, 1H), 4.91 (m, 1H), 4.11 (dd, 1H, J = 9.0 Hz, J = 11.0 Hz), 3.77 (dd, 1H, J = 2.5 Hz, J = 11.5 Hz), 2.98 (m, 1H), 1.09 (d, 3H, J = 7.0 Hz), 0.95 (d, 3H, J = 7.0 Hz) ppm. ^{13}C NMR (125 MHz, $CDCl_3$, 25 °C) δ 156.1, 152.6, 134.3, 128.6, 124.1, 122.71, 97.4, 67.3, 36.3, 29.3, 19.0, 15.7 ppm. Anal. Calcd for $C_{14}H_{15}NOS_2$: C, 60.65; H, 5.42; N, 5.05; S, 23.10. Found: C, 60.51; H, 5.37; N, 5.02; S, 22.70.

*4.2.3. Cycloadditions of **3** with acetylenic dipolarophiles **6**–**8***

To a mixture of **5** (2.8 mmol) and the dipolarophile (4.2 mmol) in CH_2Cl_2 (20 mL) were added acetic anhydride and triethylamine (1:3, 3 mL) and the reaction mixture was heated at reflux for 1 h (TLC analysis: ethyl acetate:hexane 2:1 v/v). The products were isolated by column chromatography on silica gel [Merk 60 (400-230 mesh)] using ethyl acetate and hexane (1:1 and 2:1) as eluents. The solvent was removed to dryness and the residue was treated with diethyl ether to give the thiazolopyridones **9**–**11**, which were further recrystallized from ethyl acetate.

*4.2.4. Dimethyl 5-oxo-3,5-dihydro-2H-thiazolo[3,2-a]pyridine-7,8-dicarboxylate (**9**)*

Compound **9** was obtained from **3** and **6** after 1 h. Recrystallized from ethyl acetate (15%) had mp 131–135 °C. FTIR (KBr) ν_{max} 3463, 3019, 2958, 1737, 1693, 1651, 1442, 1265, 1143, 1056, 986, 839, 786 cm^{-1}. ^{1}H NMR (500 MHz, $CDCl_3$, 25 °C) δ 6.24 (s, 1H), 4.53 (t, 2H, J = 8.0 Hz), 3.88 (s, 3H), 3.83 (s, 3H), 3.38 (t, 2H, J = 8.0 Hz) ppm. ^{13}C NMR (125 MHz, $CDCl_3$, 25 °C) δ 167.0, 164.0, 160.4, 158.9, 145.0, 113.5, 101.6, 52.8, 52.4, 50.9, 27.7 ppm. Anal. Calcd for $C_{11}H_{11}NO_5S$: C, 49.07; H, 4.10; N, 5.20; S, 12.00. Found: C, 48.90; H, 4.21; N, 5.27; S, 12.04.

*4.2.5. Methyl 5-oxo-3,5-dihydro-2H-thiazolo[3,2-a]pyridine-8-carboxylate (**10**)*

Compound **10** was obtained from **3** and **7** after 1 h. Recrystallized from ethyl acetate (37%) had mp 170–174 °C. FTIR (KBr) ν_{max} 3052, 2988, 2951, 1687, 1659, 1508, 1435, 1298, 1206, 1124, 1020, 834, 781 cm^{-1}. ^{1}H NMR (500 MHz, $CDCl_3$, 25 °C) δ 7.82 (d, 1H, J = 9.5 Hz), 6.24 (d, 1H, J = 9.5 Hz), 4.56 (t, 3H, J = 7.5 Hz), 3.83 (t, 2H, J = 7.5 Hz), 3.87 (s, 3H), 3.37 (t, 2H, J = 8.0 Hz) ppm. ^{13}C NMR (125 MHz, $CDCl_3$, 25 °C) δ 165.1, 161.9, 157.6, 139.5, 114.2, 104.5, 52.1, 50.6, 27.6 ppm. Anal. Calcd for $C_9H_9NO_3S$: C, 51.17, H, 4.29, N, 6.63, S, 15.18. Found: C, 51.12, H, 4.22, N, 6.60, S, 15.29.

*4.2.6. Ethyl 5-oxo-3,5-dihydro-2H-thiazolo[3,2-a]pyridine-8-carboxylate (**11**)*

Compound **11** was obtained from **3** and **8** after 1 h. Recrystallized from ethyl acetate (32%) had mp 112–115 °C. FTIR (KBr) ν_{max} 2958, 2925, 2854, 1697, 1640, 1511, 1443, 1412, 1293, 1128, 1035, 823, 778, 589 cm^{-1}. ^{1}H NMR (400 MHz, $CDCl_3$, 25 °C) δ 7.84 (d, 1H, J = 9.6 Hz), 6.25 (d, 1H, J = 9.2 Hz), 4.52 (t, 2H, J = 8.0 Hz), 4.33 (q, 2H, J = 7.2 Hz), 3.37 (t, 2H, J = 8.0 Hz), 1.37 (t, 3H, J = 7.2 Hz) ppm. ^{13}C NMR (100 MHz, $CDCl_3$, 25 °C) δ 164.6, 162.0, 157.3, 139.6, 114.1, 104.8, 61.2, 50.6, 27.6, 14.4 ppm. Anal. Calcd for $C_{10}H_{11}NO_3S$: C, 53.32, H, 4.92, N, 6.22, S, 14.23. Found: C, 53.12, H, 4.89, N, 6.21, S, 14.09.

Table 7
Bond lengths, Hessian eigenvalues of ρ(r), ρ(r) and ∇^2 ρ(r) for BCPs of incipient bonds C6-C7 in TS1$_{24}$ and TS1$_{25}$.

Structure	BCP	Bond lenght (Å)	Eigenvalues of Hessian of ρ(r)			ρ(r) (au)	$\nabla^2\rho$(r) (au)
TS1$_{24}$	BCP$_{C6\text{-}C7}$	1.94	0.2483	−0.1192	−0.1264	0.0976	0.0027
TS1$_{25}$	BCP$_{C6\text{-}C7}$	1.93	0.2529	−0.1241	−0.1306	0.0999	−0.0018

*4.2.7. Cycloadditions of **15** with acetylenic dipolarophiles **6**–**8***

A mixture of **15** (1.4 mmol), the dipolarophile (1.8 mmol), and toluene (25 mL) was heated at reflux until the disappearance of the orange color (TLC analysis: ethyl acetate:hexane 1:2 v/v). The solvent was evaporated to dryness and the resulting residue was suspended in methanol or ethanol to yield the corresponding pyridones (**16**–**18**), which were further recrystallized from ethyl acetate.

*4.2.8. (S)-Dimethyl 3-isopropyl-5-oxo-6-phenyl-3,5-dihydro-2H-thiazolo[3,2-a]pyridine-7,8-dicarboxylate (**16**)*

Compound **16** was obtained from **15** and **6** after 2 hRecrystallized from ethyl acetate (56%) had mp 151–153 °C. $[\alpha]_D$ 276.7° (*c* 5.2, CH_2Cl_2). FTIR (KBr) ν_{max} 2954, 2868, 1740, 1694, 1652, 1511, 1437, 1365, 1315, 1234, 1212, 1176, 716, 703, 537 cm^{-1}. ^1H NMR (500 MHz, $CDCl_3$, 25 °C) δ 7.32 (m, 5H), 5.17 (m, 1H), 3.83 (s, 3H), 3.57 (s, 3H), 3.48 (dd, 1H, $J = 9.0$ Hz, $J = 11.5$ Hz), 3.17 (dd, 1H, $J = 1.5$ Hz, $J = 12.0$ Hz), 2.58 (m, 1H), 0.99 (dd, 6H, $J = 7.0$ Hz, $J = 15.5$ Hz) ppm. ^{13}C NMR (125 MHz, $CDCl_3$, 25 °C) 166.8, 164.2, 160.3, 158.2, 142.4, 133.2, 129.7, 128.2, 128.0, 125.1, 100.8, 68.5, 52.4, 52.2, 29.3, 28.3, 19.4, 16.4 ppm. Anal. Calcd for $C_{20}H_{21}NO_5S$: C, 62.00, H, 5.46, N, 3.62, S, 8.28. Found: C, 61.86, H, 5.61, N, 3.70, S, 7.93.

*4.2.9. (S)-Methyl 3-isopropyl-5-oxo-6-phenyl-3,5-dihydro-2H-thiazolo[3,2-a]pyridine-8-carboxylate (**17**)*

Compound **17** was obtained from **15** and **7** after 2 hRecrystallized from ethyl acetate (74%) had mp 155–157 °C. $[\alpha]_D$ 361.2° (*c* 6.1, CH_2Cl_2). FTIR (KBr) ν_{max} 3052, 3032, 2995, 2962, 2868, 1696, 1640, 1520, 1446, 1425, 1367, 1301, 1237, 1182, 1104, 1015, 788, 703, 592 cm^{-1}. ^1H NMR (500 MHz, $CDCl_3$, 25 °C) δ 8.01 (s, 1H), 7.68 (m, 2H), 7.40 (m, 2H), 7.32 (m, 1H), 5.22 (m, 1H), 4.35 (m, 2H), 3.49 (dd, 1H, $J = 9.0$ Hz, $J = 11.5$ Hz), 3.19 (dd, 1H, $J = 1,5$ Hz, $J = 12.0$ Hz), 2.64 (m, 1H), 1.37 (t, 3H, $J = 7.0$ Hz) 1.03 (d, 3H, $J = 7.0$ Hz), 0.94 (d, 3H, $J = 7.0$ Hz) ppm. ^{13}C NMR (125 MHz, $CDCl_3$, 25 °C) δ 165.3, 160.6, 156.6, 137.2, 135.8, 128.4, 128.2, 127.7, 125.6, 103.8, 68.0, 52.0, 29.3, 28.3, 19.4, 16.3 ppm. Anal. Calcd for $C_{18}H_{19}NO_3S$: C, 65.63, H, 5.81, N, 4.25, S, 9.73. Found: C, 65.58, H, 5.79, N, 4.22, S, 9.55.

*4.2.10. (S)-Ethyl 3-isopropyl-5-oxo-6-phenyl-3,5-dihydro-2H-thiazolo[3,2-a]pyridine-8-carboxylate (**18**)*

Compound **18** was obtained from **15** and **8** after 2 hRecrystallized from ethyl acetate (64%) had mp 108–111 °C. $[\alpha]_D$ 326.2° (*c* 5.4, CH_2Cl_2). FTIR (KBr) ν_{max} 3065, 2961, 2935, 2873, 1694, 1639, 1596, 1521, 1445, 1395, 1303, 1255, 1237, 1168, 1102, 1035, 777, 700, 597, 542 cm^{-1}. ^1H NMR (500 MHz, $CDCl_3$, 25 °C) δ 8.02 (s, 1H), 7.68 (m, 2H), 7.41 (t, 2H, $J = 7.0$ Hz), 7.33 (m, 1H), 4.35 (m, 2H) 3.49 (dd, 1H, $J = 9.0$ Hz, $J = 11.5$ Hz), 3.20 (dd, 1H, $J = 1.0$ Hz, $J = 11.5$ Hz), 2.64 (m, 1H), 1.37 (t, 3H, $J = 7.0$ Hz), 1.03 (d, 3H, $J = 7.0$ Hz), 0.95 (d, 3H, $J = 7.0$ Hz) ppm. ^{13}C NMR (125 MHz, $CDCl_3$, 25 °C) δ 164.9, 160.6, 156.4, 137.3, 135.8, 128.5, 128.2, 127.7, 125.6, 104.2, 68.0, 61.2, 29.3, 28.3, 19.4, 16.4, 14.4 ppm. Anal. Calcd for $C_{19}H_{21}NO_3S$: C, 66.45, H, 6.16, N, 4.08, S, 9.34. Found: C, 66.39, H, 6.14, N, 3.97, S, 9.30.

Acknowledgements

Financial support from the Ministry of Economy and Competitiveness (Grant CTQ2013-44787P), and the Junta de Extremadura (*Ayuda a Grupos de Investigación*, Grant GR15022) is greatly acknowledged. We also thank *Cénits and Fundación Computaex* for allowing us the use of Supercomputer LUSITANIA.

Appendix A. Supplementary data

Supplementary data related to this article can be found at http://dx.doi.org/10.1016/j.tet.2017.01.064.

References

1. Taylor RD, MacCoss M, Lawson ADG. *J Med Chem*. 2014;57:5845–5859.
2. Vaquero JJ, Alvarez-Builla J. In: Alvarez-Builla J, Vaquero JJ, Barluenga J, eds. *Modern Heterocyclic Chemistry*. vol. 4. Weinheim: Wiley-VCH; 2011: 1989–2070. Ch. 22.
3. Pinto DJP, Smallheer JM, Cheney DL, Knabb RM, Wexler RR. *J Med Chem*. 2010;53:6243–6274.
4. Shi F, Li C, Xia M, et al. *Bioorg Med Chem Lett*. 2009;19:5565–5568.
5. (a) . In: Padwa A, Pearson WH, eds. *Synthetic Applications of 1,3-Dipolar Cycloaddition Chemistry toward Heterocycles and Natural Products*. New York: John Wiley & Sons; 2002;
(b) Pellisier H. *Tetrahedron*. 2007;63:3235–3285;
(c) Suga H, Itoh K. In: Nishiwaki N, ed. *Methods and Applications of Cycloaddition Reactions in Organic Syntheses*. Hoboken, New Jersey: John Wiley & Sons, Inc.; 2013:175–204;
(d) Hasimoto T, Maruoka K. *Chem Rev*. 2015;115:5366–5412;
(e) . In: Danheiser RL, ed. *Science of Synthesis: Houben-weyl Methods of Molecular Transformations*. Stuttgart: Georg Thieme; 2014:461–462. Compounds with Four and Three Carbon-heteroatom Bonds; vol. 23.
6. Candeias NR, Branco LG, Gois PMP, Afonso CAM, Trindade AF. *Chem Rev*. 2009;109:2703–2802.
7. (a) Ollis WD, Ramsden CA. In: Katritzky AR, Boulton AJ, eds. *Advances in Heterocyclic Chemistry*. vol. 19. New York: Academic Press; 1976:1–122;
(b) Newton CG, Ramsden CA. *Tetrahedron*. 1982;38:2965–3011;
(c) Potts KT. In: Padwa A, ed. *1,3-Dipolar Cycloaddition Chemistry*. vol. 2. New York: John Wiley & Sons; 1984:1–82;
(d) Ollis WD, Stanforth SP, Ramsden CA. *Tetrahedron*. 1985;41:2239–2329;
(e) Badami BV. *Resonance*. 2006;11:40–48.
8. (a) Osterhout MH, Nadler WR, Padwa A. *Synthesis*. 1994:123–141;
(b) Benetti S, De Risi C, Pollini GP, Zanirato V. *Chem Rev*. 2012;112:2129–2163;
(c) Lopchuk JM. In: Gribble GW, ed. *Metalation of Azoles and Related Five-membered Ring Heterocycles*. Berlin: Springer; 2012:381–413.
9. (a) Ávalos M, Babiano R, Cintas P, Jiménez JL, Palacios. *Acc Chem Res*. 2005;38: 460–468. and references cited therein;
(b) Cantillo D, Ávalos M, Babiano R, et al. *Org Lett*. 2008;10:1079–1082;
(c) Cantillo D, Ávalos M, Babiano R, et al. *J Org Chem*. 2009;74:3698–3705;
(d) Cantillo D, Ávalos M, Babiano R, Cintas P, Jiménez JL, Light ME, et al. *J Org Chem*. 2009;74:7644–7650;
(e) Sánchez B, Arévalo MJ, Bravo JL, López I, Light ME, Silvero G. *Austr J Chem*. 2009;62:356–359;
(f) Sánchez B, López I, Light ME, Silvero G, Bravo JL. *Eur J Org Chem*. 2010: 1648–1652.
10. de la Concepción J García, Ávalos M, Babiano R, Cintas P, Jiménez JL, Light ME, et al. *Tetrahedron*. 2016;72:4665–4670.
11. Delaunay D, Toupet L, Le Corre M. *J Org Chem*. 1995;60:6604–6607.
12. Crystallographic data (excluding structure factors) for the structures in this paper have been deposited with the Cambridge Crystallographic Data Centre as supplementary publication no. CCDC-1519821.
13. (a) Badenhoop JK, Weinhold F. *J Chem Phys*. 1997;107:5406–5421;
(b) ibid. 5422–5432, (c) Badenhoop JK, Weinhold F. *Int J Quantum Chem*. 1999;72:269–280.
14. Reed AE, Weinhold F. *J Chem Phys*. 1985;83:1736–1740.
15. Foster JP, Weinhold F. *J Am Chem Soc*. 1980;102:7211–7218.
16. Weinhold F. *J Comput Chem*. 2012;33:2440–2449.
17. Frisch MJ, Trucks GW, Schlegel HB, et al. *Gaussian 09, Revision D.01*. Wallingford, CT: Gaussian, Inc.; 2009.
18. Zhao Y, Truhlar DG. *Theor Chem Acc*. 2008;120:215–241.
19. a) Ditchfield R, Hehre WJ, Pople JA. *J Chem Phys*. 1971;54:724–728;
b) Hehre WJ, Ditchfield R, Pople JA. *Mol Phys*. 1974;27:209–214;
c) Gordon MS. *Chem Phys Lett*. 1980;76:163–168;
d) Hariharan PC, Pople JA. *Theor Chem Acc*. 1973;28:213–222;
e) Francl MM, Pietro WJ, Hehre WJ, et al. *J Chem Phys*. 1982;77:3654–3665.
20. a) Marenich AV, Cramer CJ, Truhlar DG. *J Phys Chem B*. 2009;113:4538–4543;
b) Marenich AV, Cramer CJ, Truhlar DG. *J Phys Chem B*. 2009;113:6378–6396;
c) Ribeiro RF, Marenich AV, Cramer CJ, Truhlar DG. *J Comput.-Aided Mater*. 2010;24:317–333;
d) Halim MA, Shaw DM, Poirier RA. *J Mol Struct*. 2010;960:63–72;
e) Saielli G. *J Phys Chem A*. 2010;114:7261–7265.
21. Glendening ED, Badenhoop JK, Reed AE, et al. *Theoretical Chemistry Institute*. Madison: University of Wisconsin; 2013.
22. http://www.jmol.org/.